



Full Length Article

Enhanced hydrogen storage properties of Mg by the synergistic effect of grain refinement and NiTiO₃ nanoparticles

Nianhua Yan^a, Xiong Lu^a, Zhiyu Lu^a, Haijie Yu^a, Fuying Wu^b, Jianguang Zheng^a,
Xiuzhen Wang^a, Liuting Zhang^{a,*}

^aSchool of Energy and Power, Jiangsu University of Science and Technology, Zhenjiang, 212003, China

^bAnalysis and Testing Center, Jiangsu University of Science and Technology, Zhenjiang, 212003, China

Received 11 November 2020; received in revised form 30 January 2021; accepted 30 March 2021

Available online 15 May 2021

Abstract

As a promising hydrogen storage material, the practical application of magnesium is obstructed by the stable thermodynamics and sluggish kinetics. In this paper, three kinds of NiTiO₃ catalysts with different mole ratio of Ni to Ti were successfully synthesized and doped into nanocrystalline Mg to improve its hydrogen storage properties. Experimental results indicated that all the Mg-NiTiO₃ composites showed prominent hydrogen storage performance. Especially, the Mg-NiTiO₃/TiO₂ composite could take up hydrogen at room temperature and the apparent activation energy for hydrogen absorption was dramatically decreased from 69.8 ± 1.2 (nanocrystalline Mg) kJ/mol to 34.2 ± 0.2 kJ/mol. In addition, the hydrogenated sample began to release hydrogen at about 193.2 °C and eventually desorbed 6.6 wt% H₂. The desorption enthalpy of the hydrogenated Mg-NiTiO₃-C was estimated to be 78.6 ± 0.8 kJ/mol, 5.3 kJ/mol lower compared to 83.9 ± 0.7 kJ/mol of nanocrystalline Mg. Besides, the sample revealed splendid cyclic stability during 20 cycles. No obvious recession occurred in the absorption and desorption kinetics and only 0.3 wt% hydrogen capacity degradation was observed. Further structural analysis demonstrates that nanosizing and catalyst doping led to a synergistic effect on the enhanced hydrogen storage performance of Mg-NiTiO₃-C composite, which might serve as a reference for future design of highly effective hydrogen storage materials.

© 2021 Chongqing University. Publishing services provided by Elsevier B.V. on behalf of KeAi Communications Co. Ltd.

This is an open access article under the CC BY-NC-ND license (<http://creativecommons.org/licenses/by-nc-nd/4.0/>)

Peer review under responsibility of Chongqing University

Keywords: Hydrogen storage; NiTiO₃; Nanocrystalline Mg; Reversibility; Synergistic effect.

1. Introduction

The rapid development of modern industrial civilization has caused more serious environmental pollution and energy shortage than ever before [1]. Thus, finding a clean and environment-friendly energy carrier has been a research hotspot worldwide [2,3]. Among various alternative energy sources, hydrogen is considered one of the most optimal carriers owing to the advantages of its rich reserves, high calorific value, and wide application [4–7]. To store and deliver hydrogen in a safe and efficient way, Solid-state hydrogen storage technology greatly caught scientists' attention [8–10].

Different hydrogen storage materials have been intensively studied, such as MgH₂, MgNiH₄, LiBH₄, NaBH₄, Mg(BH₄)₂, NaAlH₄, etc. [11–16]. Among them, MgH₂ has received wide attention in recent years due to its low cost, high capacity, and good reversibility [17–19]. However, the stable thermodynamics and sluggish kinetics remain key problems to its practical application in hydrogen storage [20–22].

Various modification methods for Mg-H system have been reported in literature, mainly involving nanosizing [23–26], catalyst doping [27–31] and alloying [32–34]. Refining particle size to nanoscale by ball milling is one of the most common methods for improving the kinetic properties of Mg-H system due to the high surface-to-volume ratio and short hydrogen diffusion paths. For instance, Xiao et al. [35] reported Mg₂FeH₆@MgH₂ core-shell nanostructure with particle size

* Corresponding authors at.

E-mail address: zhanglt89@just.edu.cn (L. Zhang).

of 40–60 nm could start to release H₂ at 220 °C and desorb over 5.0 wt% H₂ within 50 min at 280 °C. Moreover, the sample exhibited excellent cycling properties due to the core–shell nanostructure. In the meanwhile, Calizzi et al. [36] successfully prepared Mg–Ti nanoparticles (Mg–Ti NPs) by inert gas condensation and in situ hydrogenation at 150 °C. The calculation results showed that the values of apparent activation energy for absorption and desorption of the Mg–Ti NPs were sharply decreased to 68 kJ/mol and 78 kJ/mol, respectively.

Besides, Catalyst doping is also an effective strategy to reduce the high temperature requirement for Mg–H system. Based on previous investigations, transition metals, compounds and alloys have shown excellent catalysis to accelerate the de/rehydrogenation kinetics of MgH₂ [37,38]. Among vast transition metal catalysts been investigated, Ti-based catalysts exert superior performance. For instance, Zhang et al. [39] evidenced that 5 wt% TiO₂ nanosheet modified MgH₂ composite started to release hydrogen at 180.5 °C and the dehydrogenation activation energy was decreased to 67.6 kJ/mol. In addition, the MgH₂–5 wt% Ti₃C₂ composite prepared by Liu et al. [40] began to liberate hydrogen at 185 °C and approximately 7.1 wt% H₂ was released. Simultaneously, the dehydrogenated sample absorbed about 3.0 wt% hydrogen within 150 s at low temperature of 50 °C under 5 MPa hydrogen pressure.

As another transition metal element, Ni-based materials have also been demonstrated effective for Mg-based materials. Yao et al. [41] uniformly dispersed Ni nanoparticles on reduced graphene(Ni@rGO) and doped them into MgH₂. Experimental results showed that the onset dehydrogenation temperature of MgH₂+10 wt% Ni₄@rGO₆ was sharply decreased to 190 °C and the dehydrogenated composite could take up 5.0 wt% hydrogen in 20 min at 100 °C. Li et al. [42] also proved that nanocrystalline Ni@C greatly improved the hydrogen storage properties of MgH₂. The peak hydrogen desorption temperature of MgH₂–Ni@C composite can be reduced to 283 °C, 74 °C lower compared with that of MgH₂.

In addition, Ti-based or Ni-based bivariate materials were reported to show outstanding catalysis for MgH₂ on hydrogen storage [43–45]. Zhang et al. [43] discovered the onset dehydrogenation temperature of MgH₂–7 wt% TiNb₂O₇ was reduced to 177 °C from 300 °C (MgH₂) and about 4.5 wt% H₂ was absorbed in 3 min at 150 °C. Chen et al. [45] found MgH₂–9 NiMoO₄ absorbed 6.7 wt% hydrogen within 60 s and release 6.7 wt% hydrogen within 10 min at 300 °C. In addition, the MgH₂–9 NiMoO₄ composite exhibited excellent cycling stability and low-temperature hydrogen storage performance.

Enlightened by the previously reported modification strategies on MgH₂ including nanocrystallization and catalyst doping, three kinds of NiTiO₃ nanoparticles with different ratios of Ni to Ti were synthesized via a facile hydrothermal method and then doped into nanocrystalline Mg in this work. The Mg–NiTiO₃ composites were systematically investigated through a range of composition characterization, morphologies and hydrogen storage properties. On the basis of above experimental results and analysis, the catalytic mechanism of

Table 1
Detailed information for preparing NiTiO₃ nanoparticles.

Sample No.	C ₄ H ₁₄ NiO ₈ ·4H ₂ O	C ₁₂ H ₂₈ O ₄ Ti	Abbreviations
1	0.011 mol	0.01 mol	NiTiO ₃ -A
2	0.01 mol	0.01 mol	NiTiO ₃ -B
3	0.01 mol	0.011 mol	NiTiO ₃ -C

NiTiO₃ catalysts on MgH₂ hydrogen desorption and absorption were discussed in detail.

2. Experimental

2.1. Synthesis of NiTiO₃ nanoparticles

A typical synthesis of the NiTiO₃ catalysts were as follows: a certain amount of nickel acetate tetrahydrate (C₄H₁₄NiO₈·4H₂O, SCR, purity > 99%) and titanium tetraisopropanolate (C₁₂H₂₈O₄Ti, SCR, purity > 95%) were dissolved in 500 mL deionized water. Ammonium hydroxide (SCR, purity > 99.5%) was adopted to adjust the pH of the above solution to 11. Subsequently, the prepared solution was stirred for 24 h at room temperature. The resulting suspension was evaporated at 80 °C to get the green sediment. After the centrifugation wash (8000 rpm, 3 min) by deionized water and ethyl alcohol for several times, the green sediment was then maintained at 80 °C for 6 h to obtain the green powders. After being calcined at 800 °C for 6 h, the yellow NiTiO₃ powders were obtained. Three different NiTiO₃ nanoparticles were prepared via the above method, detailed information collected in Table 1.

2.2. Synthesis of nanocrystalline MG and MG–NiTiO₃ composite

The nanocrystalline Mg was prepared via a wet chemical ball milling method. 3 g Mg (SCR, purity > 99.9%), 0.15 mL oleamine (Sinopharm, purity > 98.5%), 0.45 mL oleic acid (Sinopharm, purity > 90%) and 6 mL n-heptane were mixed in a steel jar and subsequently milled for 40 h with the speed of 400 rpm (QM-3SP4, Nanjing Chi Shun Technology Development Co., Ltd, China). The mixture was washed with n-heptane for 3 times and the powers were collected by centrifugation (9000 rpm, 10 min). Finally, nanocrystalline Mg powers were obtained after been vacuumed at 250 °C for 3 h. 7 wt% as-prepared NiTiO₃ powers were doped into the nanocrystalline Mg by ball milling to get the composites (4 h; 400 rpm), named as Mg–NiTiO₃-A, Mg–NiTiO₃-B and Mg–NiTiO₃-C, respectively.

2.3. Characterization and measurements

In order to detect the phase compositions of the samples, X-ray diffraction (XRD) measurement was carried out on an X'Pert Pro-X-ray diffractometer (PANalytical, the Netherlands) with Cu K α radiation at 40 kV, 40 mA. Meanwhile, the

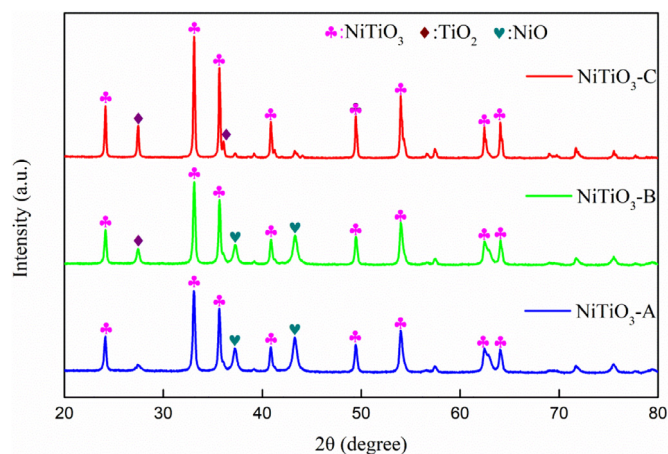


Fig. 1. XRD patterns of as-prepared NiTiO₃-A, NiTiO₃-B and NiTiO₃-C.

morphology and microstructure of the samples were characterized by Scanning Electron Microscopy (SEM, Hitachi SU-70) and Transmission Electron Microscope (TEM, Tecnai G2 F30 working at 300 kV).

A homemade Sievert's type device was employed to measure hydrogen absorption and desorption properties. For the non-isothermal mode, each sample was heated from room temperature to 400 °C under 3 MPa hydrogen pressure with a heat-up rate of 1 °C/min for hydrogen absorption. In hydrogen desorption experiment, the hydrogenated sample was heated from room temperature to 430 °C under static vacuum with a heat-up rate of 2 °C/min. With respect to the isothermal tests, each sample was rapidly heated to the desired temperature and kept for 60 min under 3 MPa hydrogen pressure (hydrogen uptake) or static vacuum environment (hydrogen release). In order to minimize errors caused by the test instruments, each experiment was repeated at least twice.

3. Results and discussion

XRD analysis of the as-prepared NiTiO₃ samples are carried out to explore the phase composition, presented in Fig. 1. It is apparent that the characteristic peaks of three samples matched well with NiTiO₃ (PDF#33-0960) at 23.8°, 32.7°, 35.4°, 40.5°, 49.1°, 53.4°, 62.0° and 63.9°. Besides, two peaks at 37.2° and 43.3° belonging to NiO occurred in NiTiO₃-A, which is due to the overdose of C₄H₁₄NiO₈. Similarly, two TiO₂ peaks at 27.3° and 36.1° occurred in NiTiO₃-C sample due to the excess amount of titanium tetraisopropanolate. Although the molar ratio of C₄H₁₄NiO₈ to C₁₂H₂₈O₄Ti is 1 to 1, the TiO₂ peak (at 27.3°) and NiO peaks (at 37.2° and 43.3°) still appeared in the NiTiO₃-B sample, which might result from the incomplete reaction during the hydrothermal or calcination process. To further reveal the morphology of the as-prepared NiTiO₃ samples, TEM measurement was employed. The TEM images in Fig. 2 indicated that the particle size of all the three NiTiO₃ was about 50 - 100 nm. Besides, it's obvious that comparing to aggregated NiTiO₃-A and NiTiO₃-B, well scattered NiTiO₃-C particles were found

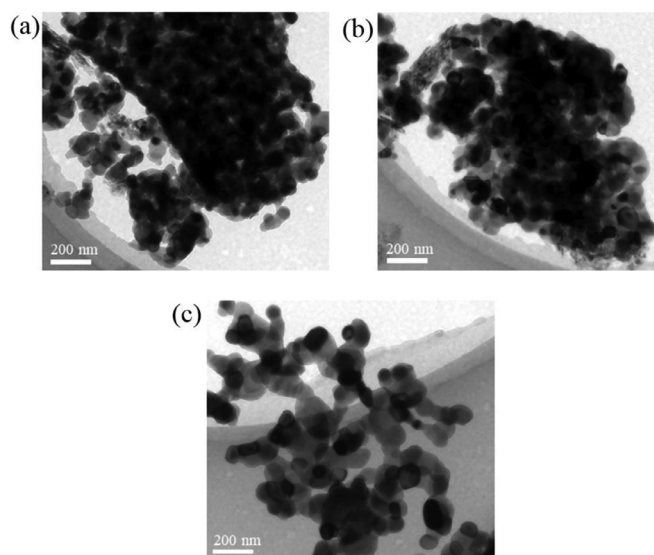


Fig. 2. TEM images of as-prepared NiTiO₃-A (a), NiTiO₃-B (b) and NiTiO₃-C (c).

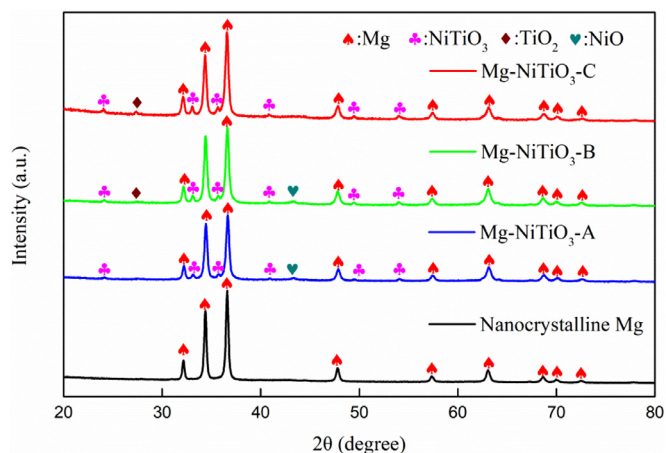


Fig. 3. XRD patterns of as-prepared nanocrystalline Mg, Mg-NiTiO₃-A, Mg-NiTiO₃-B and Mg-NiTiO₃-C.

by TEM observations, and this difference in dispersity may help the homogeneous dispersion of NiTiO₃-C nanoparticles on the surface of Mg to exert better catalytic effect.

In order to test the catalytic effect of as-prepared NiTiO₃, 7 wt% as-prepared NiTiO₃ powers were doped into the nanocrystalline Mg by ball milling. Fig. 3 shows the XRD patterns of different NiTiO₃ doped Mg samples. No detectable impurities can be found in the diffraction peaks of nanocrystalline Mg, which means no detectable oxidation of Mg appeared during the preparation process. For the Mg-NiTiO₃-A, Mg-NiTiO₃-B and Mg-NiTiO₃-C composites, both the strong Mg phase and obvious reflection signals of NiTiO₃ could be detected. Besides, some weak signals from NiO and TiO₂ can also be observed, which are in consist with Fig. 2. Based on the Scherrer formula and XRD data, the average crystallite size of the above samples can be calculated to be 64.4 nm (nanocrystalline Mg), 54.6 nm (Mg-NiTiO₃-A), 52.5 nm (Mg-NiTiO₃-B) and 47.5 nm (Mg-NiTiO₃-C), respectively. This

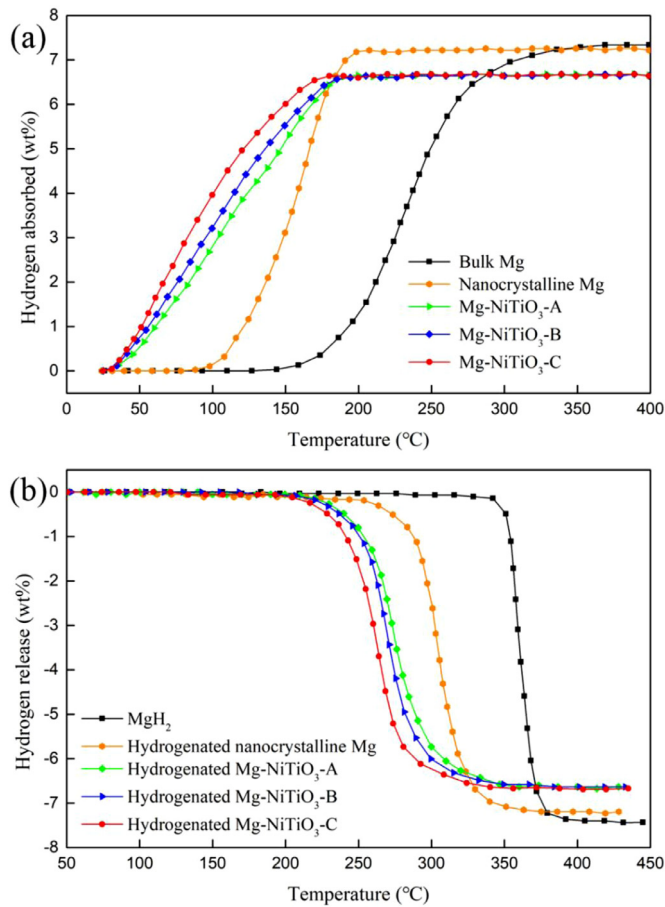


Fig. 4. The curves of no-isothermal hydrogen uptake for Mg-NiTiO₃-A, Mg-NiTiO₃-B, Mg-NiTiO₃-C, nanocrystalline Mg and bulk Mg (a); the curves of no-isothermal hydrogen release for hydrogenated Mg-NiTiO₃-A, Mg-NiTiO₃-B, Mg-NiTiO₃-C, nanocrystalline Mg and MgH₂ (b).

indicates that doping of NiTiO₃, especially NiTiO₃-C with higher Ti amount, may significantly reduce the grain size of nanocrystalline Mg.

Fig. 4a shows the curves of no-isothermal hydrogen uptake for the Mg-NiTiO₃-A, Mg-NiTiO₃-B, Mg-NiTiO₃-C, nanocrystalline Mg and bulk Mg samples. The bulk Mg started to take up H₂ at about 146.5 °C while the nanocrystalline Mg could begin to absorb H₂ at about 87.6 °C. Both samples could obtain a hydrogen absorption capacity of approximate 7.2 wt%. It could be told that nano-sized Mg show better hydrogen uptake performance. After NiTiO₃-A, NiTiO₃-B and NiTiO₃-C were doped, all the three Mg-NiTiO₃ samples started to absorb H₂ from room temperature with a final capacity of 6.6 wt%. Besides, the distinctions on hydrogen absorption rate for the three doped samples were also clearly observed as follows: Mg-NiTiO₃-C > Mg-NiTiO₃-B > Mg-NiTiO₃-A. In addition, the non-isothermal hydrogen release curves of the hydrogenated samples shown in Fig. 4b revealed that bulk Mg started to desorb hydrogen at about 347.5 °C while the hydrogenated nanocrystalline Mg began to release H₂ at about 262.4 °C, with a hydrogen desorption capacity of 7.2 wt% for both samples. As expected, the

three NiTiO₃ doped samples started to desorb hydrogen at about 206.1 °C (Mg-NiTiO₃-A), 199.6 °C (Mg-NiTiO₃-B) and 193.2 °C (Mg-NiTiO₃-C), respectively. Besides, the dehydrogenation kinetics of hydrogenated Mg-NiTiO₃-C was better than that of hydrogenated Mg-NiTiO₃-B and Mg-NiTiO₃-A, which is in agreement with the absorption kinetics. Above investigation results on the hydrogen absorption and desorption demonstrated that the formation of nanocrystalline Mg and further doping of NiTiO₃ nanocatalysts remarkably enhanced the hydrogen storage performance in Mg-MgH₂ system. In addition, the Mg-NiTiO₃-C composite shows superior hydrogen absorption and desorption properties compared with those of Mg-NiTiO₃-A and Mg-NiTiO₃-B composites, thus, the Mg-NiTiO₃-C composite was chosen in the following experiments and discussions.

The hydrogen absorption kinetic of Mg-NiTiO₃-C sample was further investigated by isothermal hydrogenation measurements. Fig. 5a and Fig. 5b reveal the isothermal hydrogen uptake curves for nanocrystalline Mg and Mg-NiTiO₃-C, respectively. Nanocrystalline Mg showed partial hydrogen absorption capacities (1.5 wt% at 150 °C; 3.7 wt% at 175 °C; 6.3 wt% at 200 °C) within the first 10 min. Encouragingly, 2.7 wt% and 1.7 wt% hydrogen was absorbed in Mg-NiTiO₃-C composite within the first 10 min at temperatures as low as 125 °C and 100 °C, respectively, superior than that of nanocrystalline Mg at 150 °C. Moreover, when the hydrogenation temperature was decreased to 75 °C, the Mg-NiTiO₃-C sample could still absorb about 1 wt% hydrogen within the first 10 min and over 2 wt% hydrogen was taken up in 30 min. At 150 °C, the nanocrystalline Mg absorbed about 5 wt% H₂ in 60 min while over 6 wt% H₂ was recharged by the Mg-NiTiO₃-C in identical time. When the preset temperature reached 175 °C and 200 °C, both the two samples showed remarkable hydrogen absorption kinetics, resulting from the high temperature.

Moreover, the apparent activation energy (E_a) for hydrogen absorption was calculated to further study the kinetic properties of the nanocrystalline Mg and Mg-NiTiO₃-C composite. The data during the isothermal hydrogen uptake for each sample (Fig. 5a and Fig. 5b) was simulated through the Johnson-Mehl-Avrami-Kolmogorov (JMAK) equation [46]. The expression and relevant parameters for the JMAK equation are shown in the following equation.

$$\ln [-\ln(1 - \alpha)] = n \ln k + n \ln t \quad (1)$$

Where α is the proportion of Mg transformed into MgH₂, k represents an effective kinetic parameter, t means t moment and n denotes the Avrami exponent, respectively. And the values of n and $n \ln k$ were obtained by fitting the JMAK plots, shown in Fig. 5c and Fig. 5d. Subsequently, the values of E_a for hydrogen absorption were acquired according to the Arrhenius equation [47], which is displayed as follows:

$$k = A \exp(-E_a/RT) \quad (2)$$

As depicted in Fig. 5e, the calculated E_a values for hydrogen absorption of the nanocrystalline Mg and Mg-NiTiO₃-C were 69.8 ± 1.2 kJ/mol and 34.2 ± 0.2 kJ/mol, much lower

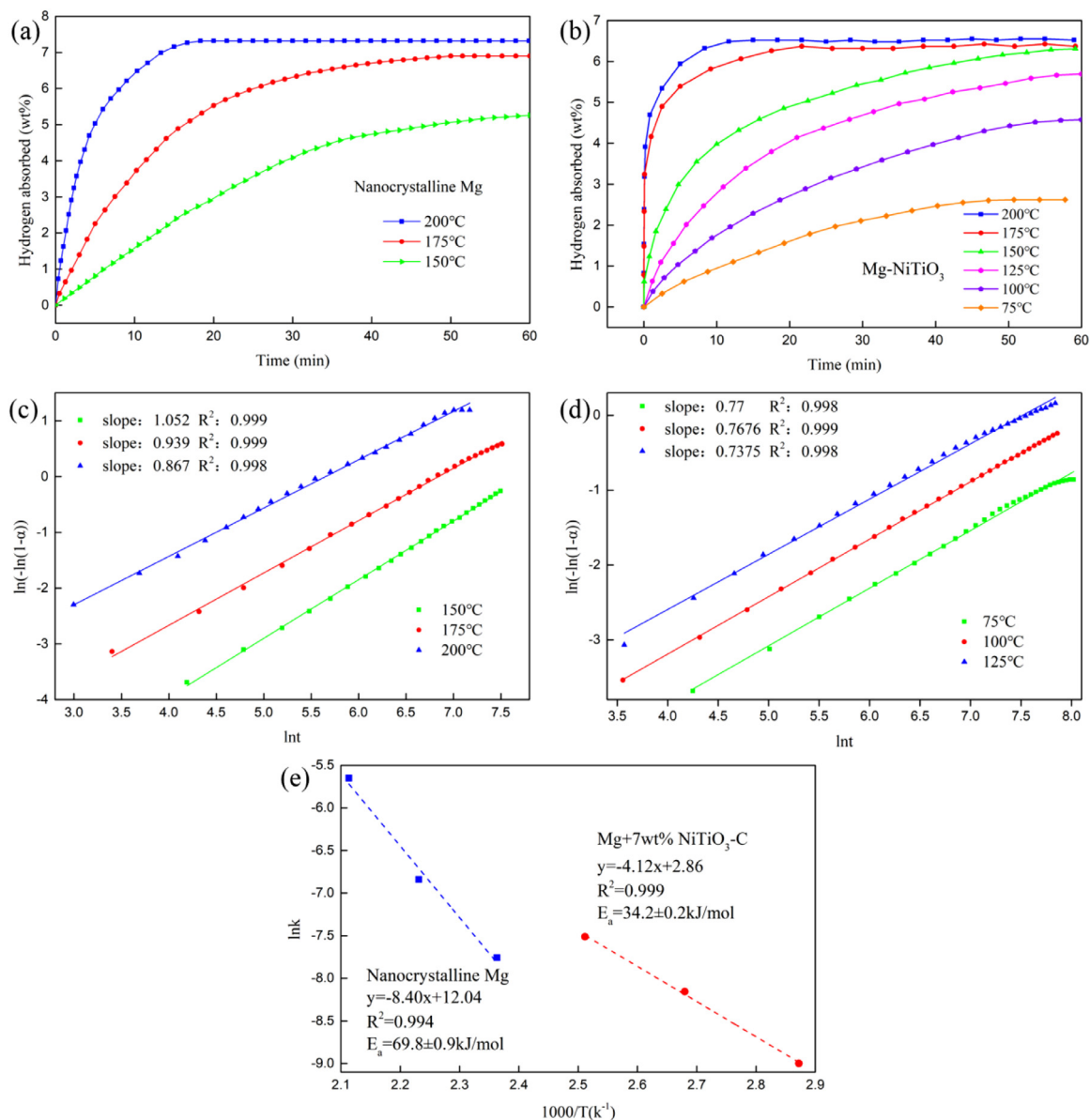


Fig. 5. Isothermal hydrogen uptake curves for the nanocrystalline Mg (a) and the Mg-NiTiO₃-C (b); isothermal hydrogenation JMAK curve plots of nanocrystalline Mg (c) and Mg-NiTiO₃-C (d); and the corresponding Arrhenius plots (e) of nanocrystalline Mg and Mg-NiTiO₃-C.

than that of MgH₂ (121.5 kJ/mol). The E_a of hydrogen absorption for the Mg-NiTiO₃-C composite was dramatically reduced about 51% (35.6 kJ/mol), compared with that of the nanocrystalline Mg, which embodied the remarkable improvement of the NiTiO₃-C on hydrogen absorption kinetics for Mg-H system.

To validly manifest the improvements on hydrogenation kinetics of Mg-NiTiO₃-C, the apparent activation energy (E_a) values of hydrogen absorption for different modified Mg-H system in recent literature were listed in Table 2. It is simply found that E_a of hydrogen absorption can be significantly reduced by various modification methods. Interestingly, the Mg-NiTiO₃-C in this paper is at state-of-the-art level of reported E_a , indicative of superior synergistic catalytic effect of

NiTiO₃-C on the hydrogen absorption kinetics property for the Mg-H system.

In addition, the hydrogen desorption kinetic property of the Mg-NiTiO₃-C composite was investigated. Fig. 6a and Fig. 6b display the isothermal hydrogen release curves for the hydrogenated nanocrystalline Mg and Mg-NiTiO₃-C, respectively. Obviously, at 325 °C, the hydrogenated nanocrystalline Mg could release 6.5 wt% H₂ within first 15 min while it only took 5 min for the hydrogenated Mg-NiTiO₃-C to desorb the same amount of hydrogen. At 300 °C, the hydrogenated Mg-NiTiO₃-C could desorb about 6.4 wt% hydrogen within the first 10 min while less than 3 wt% hydrogen was released for the hydrogenated nanocrystalline Mg at identical time. In addition, the isothermal hydrogen release curves at 275 °C for

Table 2

The apparent activation energy (E_a) of hydrogen absorption for different Mg-based samples.

No.	Sample	E_a (kJ/mol)	References
1	MgH ₂	121.5	[48]
2	MgH ₂ -10 wt% TiO ₂ @C	38.0	[49]
3	Mg-Ti-H (46 at% Ti) nanocomposite	43	[50]
4	MgH ₂ -10 wt% Zr _{0.4} Ti _{0.6} Co ₂	35.8	[51]
5	Mg@Ti	67.1	[52]
6	Mg@Ti@Ni	60.0	[52]
7	Mg nanoparticles confined in carbon aerogels	29.4	[53]
8	Mg nanowires (30–50 nm diameter)	33.5	[54]
9	Nanocrystalline Mg	69.8	This work
10	Mg-NiTiO ₃ -C	34.2	This work

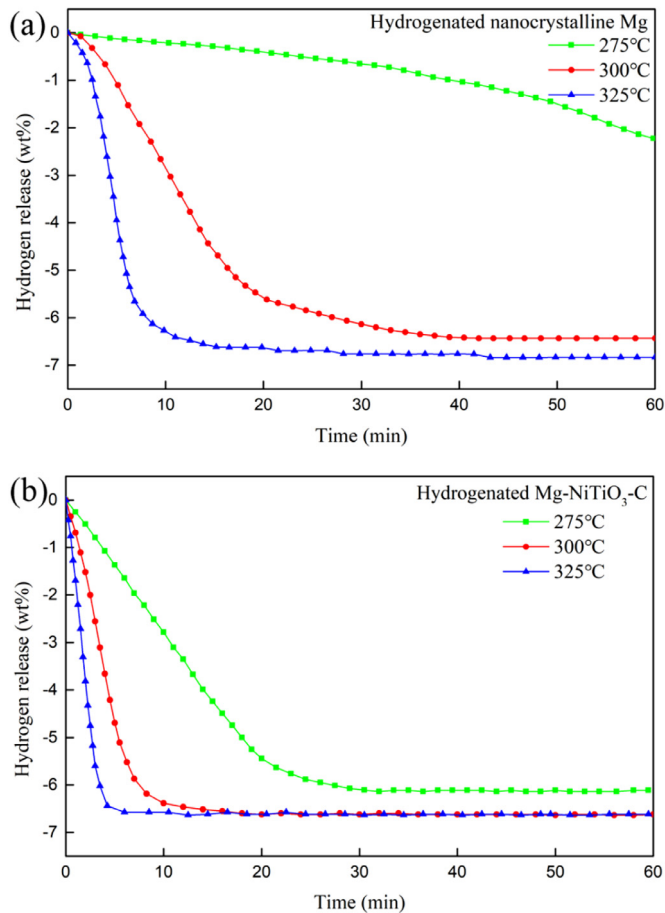


Fig. 6. The isothermal hydrogen release curves for hydrogenated nanocrystalline Mg (a) and Mg-NiTiO₃-C (b).

the two samples showed a tremendous distinction. Specifically, within the first 30 min, the hydrogenated Mg-NiTiO₃-C released about 6 wt% H₂, more than three times that of the hydrogenated nanocrystalline Mg. The above analysis demonstrated that NiTiO₃-C can serve as a bidirectional catalyst on improving the de/rehydrogenation properties of Mg.

To investigate the thermodynamic properties of hydrogenated Mg-NiTiO₃-C composite, PCT desorption curves at 300°C, 325°C and 350°C for the hydrogenated nanocrystalline Mg and Mg-NiTiO₃-C were measured. In the mean-

while, apparent pressure plateaus were detected at preset temperatures, presented in Fig. 7a and 7b. The plateau pressures of hydrogenated Mg-NiTiO₃-C were determined to be 1.52, 3.00 and 5.75 bar while that of hydrogenated nanocrystalline Mg was measured to be 1.36, 2.83 and 5.67 bar for 300°C, 325°C and 350°C, respectively. As a result, the desorption enthalpy of the hydrogenated Mg-NiTiO₃-C was estimated to be 78.6 ± 0.8 kJ/mol through the fitting the van't Hoff plot (Fig. 7c and 7d), 5.3 kJ/mol lower compared to 83.9 ± 0.7 kJ/mol of nanocrystalline Mg. The decreased value in the desorption enthalpy manifests that the addition of NiTiO₃-C could also tune the thermodynamic properties of nanocrystalline Mg.

Apart from the performances on hydrogen absorption and desorption, the reversibility is also considered as one of the most essential factors for the practical application of hydrogen storage materials [55,56]. Thus, the cycling performance of the doped sample was measured through repeating the hydrogen absorption and desorption tests for 20 cycles at 300°C under 3 MPa hydrogen pressure (absorption) and static vacuum (desorption). Fig. 8a depicts the hydrogen absorption and desorption curves in 20 cycles, which indicates inconspicuous recession occurred in the kinetic and capacity after 20 cycles. In order to observe the recession of hydrogen storage capacity more intuitively for the Mg-NiTiO₃-C composite in 20 cycles, the graph about the reversible hydrogen capacity of uptake or release for the 20 cycles were drawn and shown in Fig. 8b. Obviously, the results certify that the hydrogen capacity of the Mg-NiTiO₃-C sample after 20 cycles was 6.38 wt%, equivalent to 95.7% of the original hydrogen storage capacity (6.6 wt%). In general, MgH₂ particles tend to grow and aggregate during the thermolysis, which leads to the degenerating cycling properties [57,58]. The above results manifested that the Mg-NiTiO₃-C composite showed a superior cyclic stability. Previous studies have reported that doping Ti-based materials can improve the cycling stability for Mg-H system. Acosta et al. [59] measured the cycling hydrogen absorption and desorption curves within the first 15 min for MgH₂+5mol% Early Transition Metals (ETM=Sc, Y, Ti, Zr, V, and Nb) during 20 cycles at 300°C. The results showed that the absorption and desorption kinetics of Ti doped sample remained the most stable on cycling among the above samples. In this paper, thanks to the element Ti in NiTiO₃-C catalyst, the cyclic stability on hydrogen absorption and desorption of the Mg-NiTiO₃-C composite was similarly enhanced.

To shed light on the catalytic mechanism behind the dramatically improved hydrogen storage properties of Mg-NiTiO₃-C composite, XRD, TEM, HRTEM and EDS were carried out. Fig. 9a and Fig. 9b present the XRD profiles of as-prepared nanocrystalline Mg and Mg-NiTiO₃-C in ball milled state, hydrogenated state and dehydrogenated state, respectively. It could be apparently observed that the diffraction peaks of Mg completely dominated the ball milling state as well as the dehydrogenation state, and all the intense peaks in the hydrogenation state were belonging to MgH₂. In addition, Mg²⁺ (1305.3 eV in Mg1s) was detected from XPS

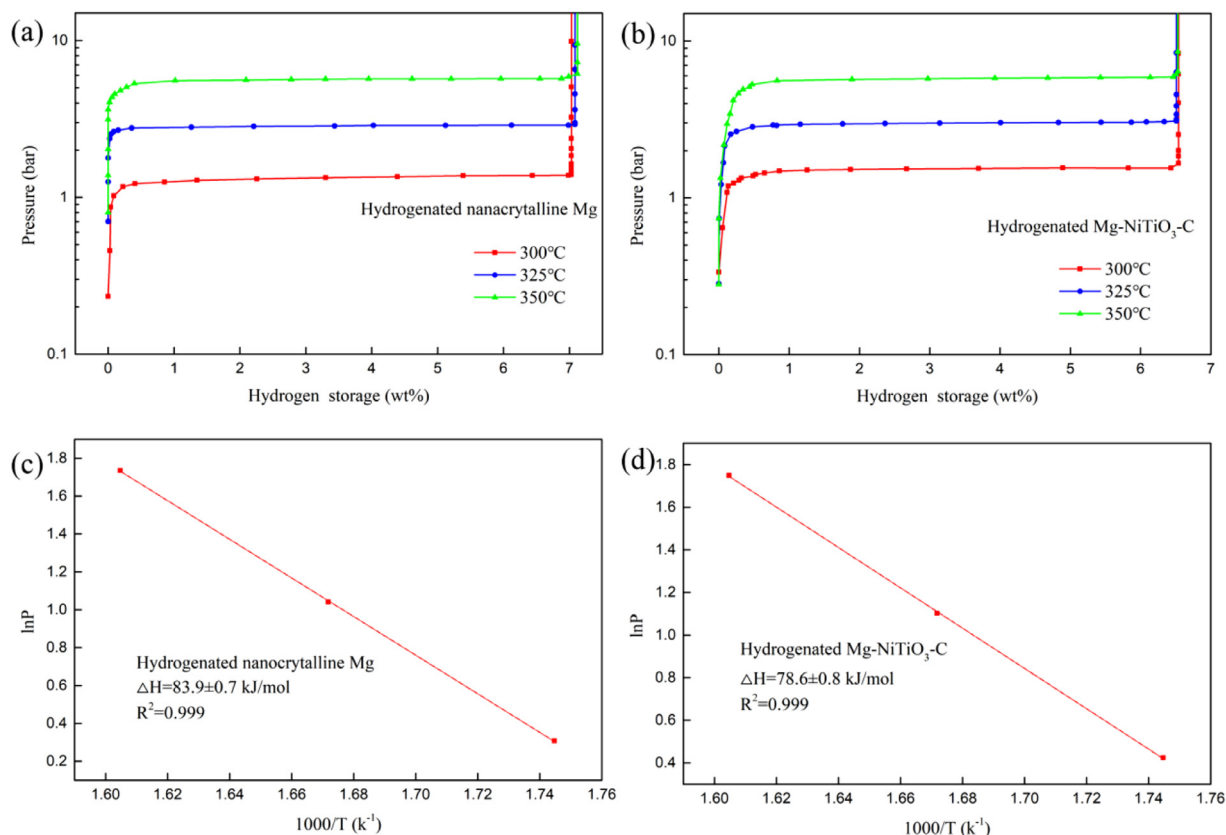


Fig. 7. PCT curves of hydrogenated nanocrystalline Mg (a) and Mg-NiTiO₃-C (b), van't Hoff plot for hydrogenated nanocrystalline Mg (c) and Mg-NiTiO₃-C (d).

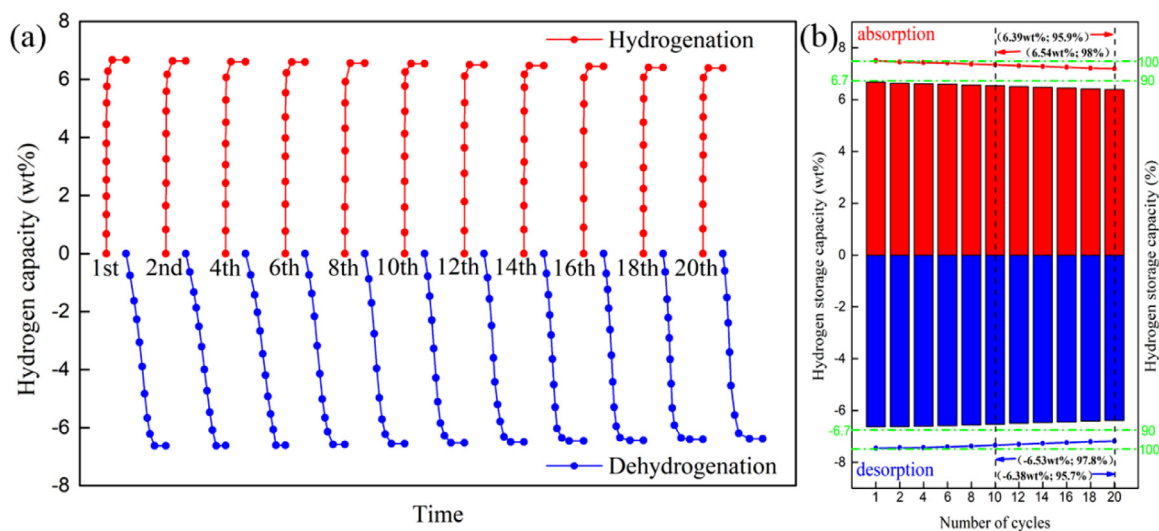


Fig. 8. The curves of hydrogen absorption and desorption during 20 cycles for Mg-NiTiO₃-C at 300 °C (a) and corresponding capacity retention graph (b).

profile of Mg-NiTiO₃-C after ball milling (Fig. S1), manifesting the existence of MgO in the surface of Mg-NiTiO₃-C. The phase of NiTiO₃ stably existed in above three states while the weak peak of TiO₂ disappeared after hydrogen absorption, which may due to the strong peak of MgH₂ at 27.9° covered the weak peak of TiO₂ at 27.3°. In the meanwhile, the lattice spacing of the (103) plane of TiO₂ was confirmed in

the TEM (Fig. 10a) and HRTEM (Fig. 10b) of hydrogenated Mg-NiTiO₃-C, which demonstrated TiO₂ still existed in hydrogenated Mg-NiTiO₃-C. Besides, TEM and HRTEM images (Fig. 10a and Fig. 10b) of the hydrogenated Mg-NiTiO₃-C confirmed the lattice spacing of the (110) plane of MgH₂ and (104) plane of NiTiO₃, which agrees well with the XRD results. Furthermore, the EDS mapping results revealed that the

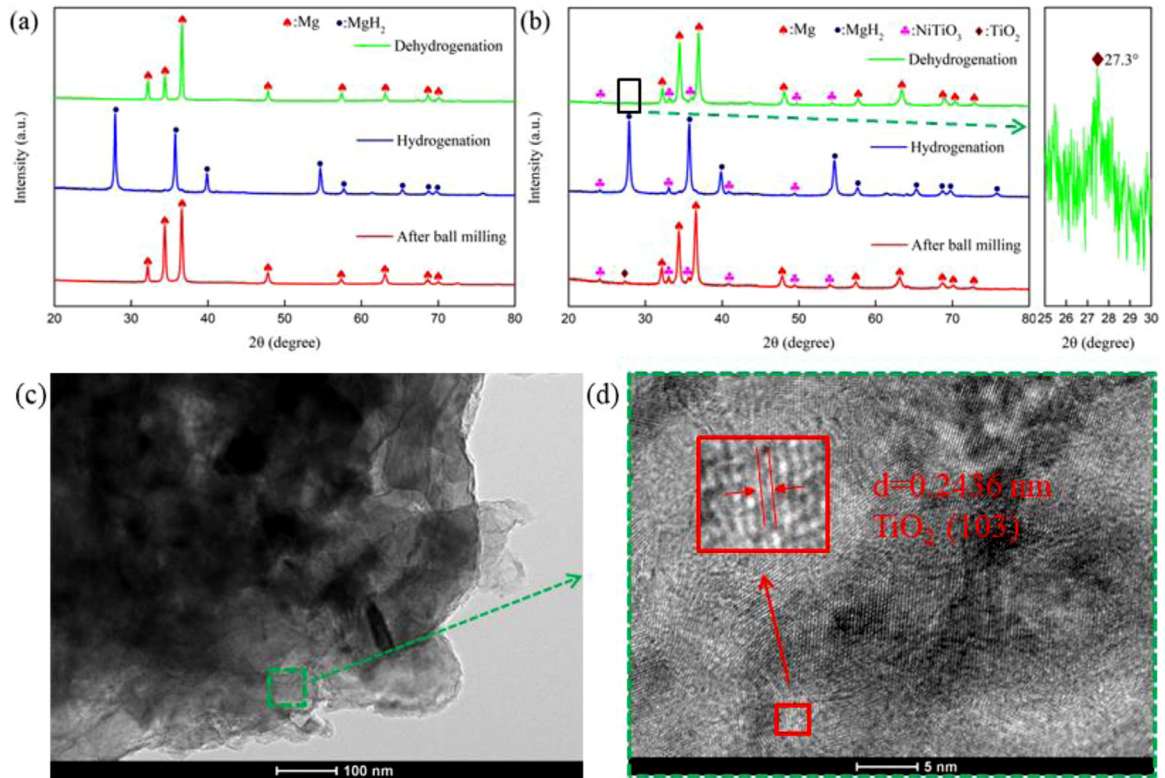


Fig. 9. X-ray diffraction patterns of as-prepared nanocrystalline Mg (a) and Mg-NiTiO₃-C (b) in the ball milling, hydrogenation and dehydrogenation states; TEM (c) and HRTEM (d) of hydrogenated Mg-NiTiO₃-C.

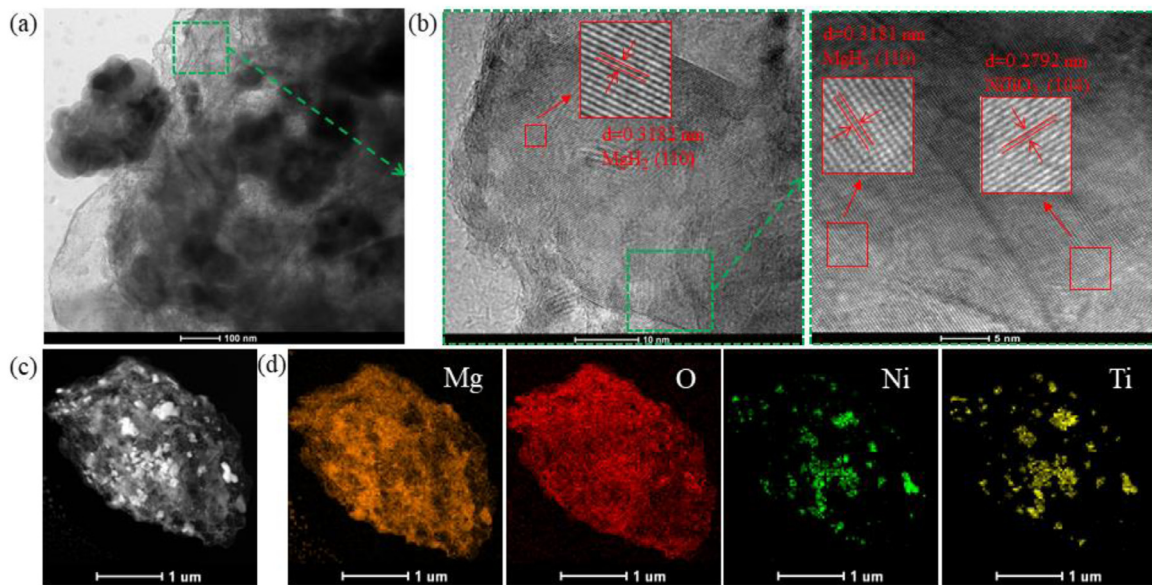


Fig. 10. TEM (a), HRTEM (b), STEM-HAADF (c) and corresponding EDS mapping results (d) of hydrogenated Mg-NiTiO₃-C.

elements of Ni, Ti, and O were evenly dispersed over MgH₂, manifesting the homogeneous distribution of NiTiO₃-C on the surface of the hydrogenated nanocrystalline Mg.

After having a total realization on the hydrogen storage property and structural changes during de/rehydrogenation in nano scale, the overall catalyzing effect of NiTiO₃-C nanoparticles could be explained in three aspects. First, TiO₂ and

NiTiO₃ themselves, as transition metal based catalysts, have previously been certified to dramatically improve the hydrogen storage performance for Mg-H system in many reports [39,49,60]. Second, the grain refinement has been reported to play a significant role for facilitating fast hydrogen absorption and desorption [61,62]. Recently, Karst et al. [63] found that nucleation of MgH₂ started at Mg grain boundaries and an

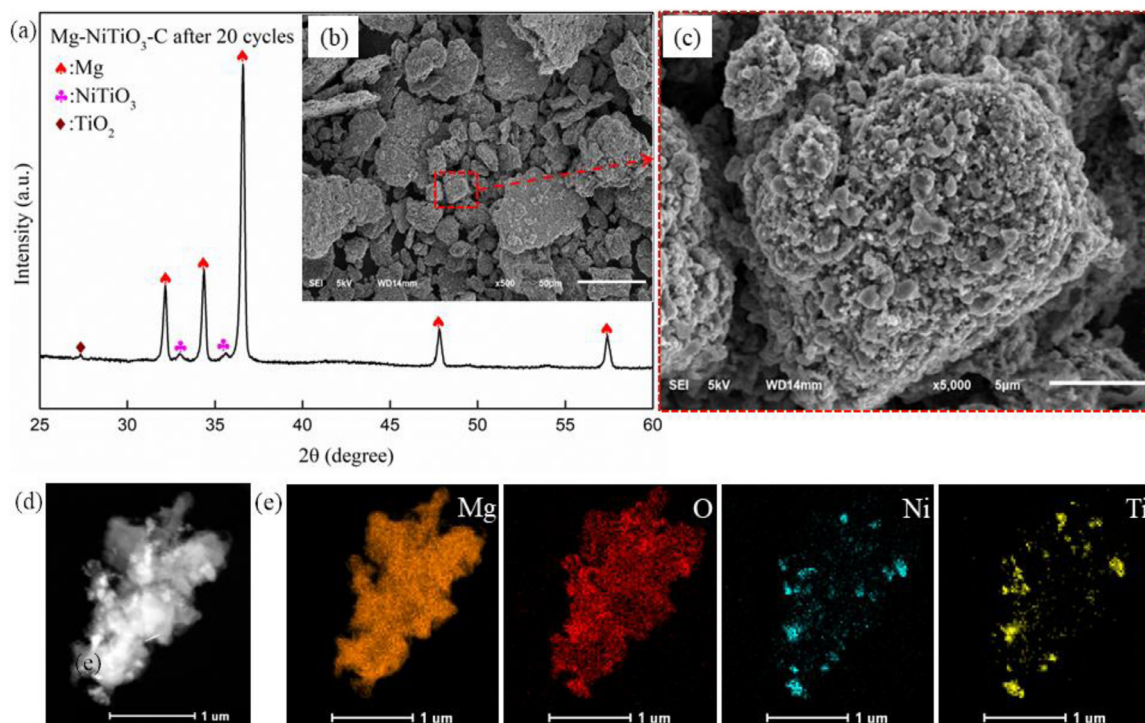


Fig. 11. XRD pattern (a), SEM images (b-c), STEM-HAADF image (d) and corresponding EDS mapping results (e) of Mg-NiTiO₃-C composite after 20 cycles.

increased grain boundary density should speed up the overall hydrogenation process. In this paper, the Mg-NiTiO₃-C composite has large grain boundary density due to the small grain size of 47.5 nm, benefiting the process of hydrogen absorption/desorption.

In the last aspect of micro morphology, Fig. 11 shows the XRD, SEM and EDS mapping of the Mg-NiTiO₃-C composite after 20 cycles. From the XRD pattern in Fig. 11a, the strong peaks of Mg and NiTiO₃ are clearly observed in the Mg-NiTiO₃-C composite after 20 cycles. In addition, a weak peak of TiO₂ is detected at about 27.3° in the composite, indicating TiO₂ still existed after 20 cycles. According to the SEM images, it is clearly observed that numerous small particles around 100 nm anchored on the surface of big particles. The EDS data verified that the small particles were NiTiO₃ and elements of Ni, Ti, and O were still uniformly distributed on the surfaces of Mg particles after 20 cycles, which prevented the sintering and agglomeration of Mg/MgH₂ during cycling, resulting in the enhanced cycling stability of Mg-NiTiO₃-C composite.

Through the above analysis and discussion, it can be concluded that the significantly enhanced hydrogen storage of Mg-NiTiO₃-C composite could be attributed to a synergistic catalyzing effect between the small grain sizes of nanocrystalline Mg and the superior catalytic effect of uniformly dispersed NiTiO₃-C. In cycling, a multivalent multielement catalytic environment consisted of Ti and Ni was formed in the Mg/MgH₂ nano system, which facilitated the dissociation and recombination of H-H and Mg-H [43,45]. Hence, the catalytic mechanism of NiTiO₃-C on hydrogen storage

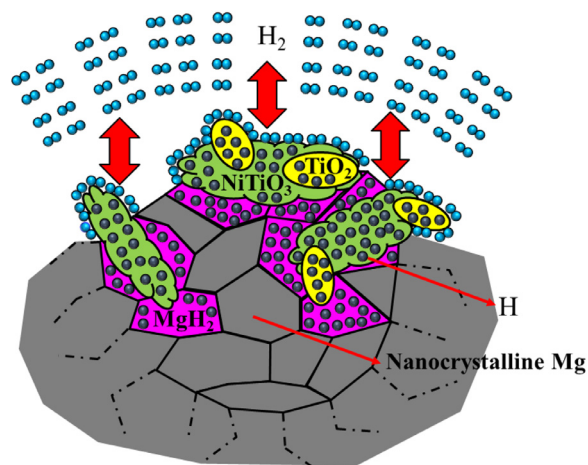


Fig. 12. Schematic diagram of catalytic mechanism on hydrogen storage for the Mg-NiTiO₃-C composite.

process for nanocrystalline Mg is proposed in Fig. 12: Numerous NiTiO₃-C particles are homogeneously anchored on the surface of Mg particles during the ball milling process. In the hydrogenation process, H₂ molecules are easily dissociated to H atoms through NiTiO₃-C and combined with Mg at a large scale of grain boundaries to promote the formation of MgH₂.

4. Conclusion

In summary, three kinds of NiTiO₃ particles were synthesized via a facile hydrothermal method and then applied in

catalyzing the as-prepared nanocrystalline Mg. The NiTiO₃-C with average particle size ranging from 50 to 100 nm and optimal particle dispersity was demonstrated to exhibit superior catalysis in facilitating the hydrogen storage properties of nanocrystalline Mg. The hydrogen uptake tests results revealed that the Mg-NiTiO₃-C composite started to absorb hydrogen at room temperature and over 4 wt% H₂ was absorbed even at 100 °C in 60 min under 3 MPa hydrogen pressure. Moreover, the E_a of hydrogen absorption for the composite was calculated to be 34.2 kJ/mol, 51% and 72% lower compared to that of the nanocrystalline Mg and bulk Mg, respectively. In addition, the hydrogenated Mg-NiTiO₃-C composite could release H₂ at 193.2 °C and complete dehydrogenation at 325 °C in 5 min with a decreased desorption enthalpy of 78.6 ± 0.8 kJ/mol. Besides, the superficial NiTiO₃ helped prevent the sintering and agglomeration of Mg/MgH₂ during de/rehydrogenation, resulting in a relatively stable cycling stability during the 20 cycles. The significantly enhanced hydrogen storage performance of Mg-NiTiO₃-C composite could be attributed to the synergistic effect between catalyzing and grain refinement. In brief, our findings may provide reference for the investigation on synergistic modification of Mg/MgH₂ system in future.

Declaration of competing interest

There is no conflict to declare.

Acknowledgements

The authors would like to acknowledge financial support from the National Natural Science Foundation of China (Grant No. 51801078), the Natural Science Foundation of Jiangsu Province (Grant No. BK20180986) and the Post-graduate Research & Practice Innovation Program of Jiangsu Province (SJCX19_0614).

Supplementary materials

Supplementary material associated with this article can be found, in the online version, at doi:10.1016/j.jma.2021.03.014.

References

- [1] I.P. Jain, C. Lal, A. Jain, *Int. J. Hydrogen Energ.* 35 (2010) 5133–5144.
- [2] L. Ouyang, Z. Cao, H. Wang, R. Hu, M. Zhu, *J. Alloy Compd.* 691 (2017) 422–435.
- [3] M. Ismail, M.S. Yahya, N.A. Sazelee, N.A. Ali, F.A.H. Yap, et al., *J. Magnes. Alloy* 8 (2020) 832–840.
- [4] K.J. Jeon, H.R. Moon, A.M. Ruminiski, B. Jiang, C. Kisielowski, et al., *Nat. Mater.* 10 (2011) 286–290.
- [5] M. Masjedi-Arani, M. Salavati-Niasari, *Int. J. Hydrogen Energ.* 42 (2017) 12420–12429.
- [6] D. Chen, Y. Xu, B. Hu, C. Yan, L. Lu, *Energ. Convers. Manage.* 171 (2018) 807–814.
- [7] J.O. Abe, A.P.I. Popoola, E. Ajenifuja, O.M. Popoola, *Int. J. Hydrogen Energ.* 44 (2019) 15072–15086.
- [8] H. Zhang, G. Xia, J. Zhang, D. Sun, Z. Guo, et al., *Adv. Energy Mater.* 8 (2018) 1702975.
- [9] X. Chen, J. Zou, X. Zeng, W. Ding, *J. Alloy Compd.* 701 (2017) 208–214.
- [10] Y. Bai, Z. Pei, F. Wu, C. Wu, *ACS Appl. Mater. Inter.* 10 (2018) 9514–9521.
- [11] T. Sadhasivam, H.T. Kim, S. Jung, S.-H. Roh, J.H. Park, et al., *Renew. Sust. Energ. Rev.* 72 (2017) 523–534.
- [12] X.Q. Tran, S.D. McDonald, Q. Gu, T. Yamamoto, K. Shigematsu, et al., *J. Power Sources* 341 (2017) 130–138.
- [13] A. Gasnier, M. Luguet, A.G. Pereira, H. Troiani, G. Zampieri, et al., *Carbon N Y* 147 (2019) 284–294.
- [14] U.B. Demirci, P. Miele, *Energ. Environ. Sci.* 2 (2009) 627–637.
- [15] M.A. Wahab, Y. Jia, D. Yang, H. Zhao, X. Yao, *J. Mater. Chem. A* 1 (2013) 3471–3478.
- [16] X. Zhang, Z. Ren, X. Zhang, M. Gao, H. Pan, et al., *J. Mater. Chem. A* 7 (2019) 4651–4659.
- [17] J. Liu, Y. Fu, W. Huang, H. Wang, L. Ouyang, et al., *J. Phys. Chem. C* 124 (2020) 6571–6579.
- [18] H. Liu, P. Sun, R.C. Bowman, Z.Z. Fang, Y. Liu, et al., *J. Power Sources* 454 (2020) 227936.
- [19] J.C. Crivello, B. Dam, R.V. Denys, M. Dornheim, D.M. Grant, et al., *Appl. Phys. A-Mater.* 122 (2016) 97.
- [20] L.Z. Ouyang, X.S. Yang, M. Zhu, J.W. Liu, H.W. Dong, et al., *J. Phys. Chem. C* 118 (2014) 7808–7820.
- [21] D. Khan, J. Zou, S. Panda, W. Ding, *J. Phys. Chem. C* 124 (2020) 9685–9695.
- [22] K.C. Kim, *Int. J. Energ. Res.* 42 (2018) 1455–1468.
- [23] M.S. El-Eskandarany, E. Shaban, A.A. Alsairafi, *Energy* 104 (2016) 158–170.
- [24] J. Zhang, Y. Zhu, H. Lin, Y. Liu, Y. Zhang, et al., *Adv. Mater.* 29 (2017) 1700760.
- [25] Q. Luo, J. Li, B. Li, B. Liu, H. Shao, et al., *J. Magnes. Alloy* 7 (2019) 58–71.
- [26] Jun Lu, Young Joon Choi, Zhigang Zak Fang, Hong Yong Sohn, E. Ronnebro, *J. Am. Chem. Soc.* 131 (2009) 15843–15852.
- [27] Y. Liu, Z. Ren, X. Zhang, N. Jian, Y. Yang, et al., *Energy Technol-Ger6* (2018) 487–500.
- [28] R. Shi, J. Zhang, Y. Zhu, Y. Liu, X. Hu, et al., *Energ. Fuel* 34 (2020) 10232–10240.
- [29] L. Zhang, Z. Cai, Z. Yao, L. Ji, Z. Sun, et al., *J. Mater. Chem. A* 7 (2019) 5624–5634.
- [30] M. Zhang, X. Xiao, B. Luo, M. Liu, M. Chen, et al., *J. Energ. Chem.* 46 (2020) 191–198.
- [31] P. Meena, R. Singh, V.K. Sharma, I.P. Jain, *J. Magnes. Alloy* 6 (2018) 318–325.
- [32] H. Yong, S. Guo, Z. Yuan, Y. Qi, D. Zhao, et al., *J. Mater. Sci. Technol.* 51 (2020) 84–93.
- [33] H.X. Huang, J.G. Yuan, B. Zhang, J.G. Zhang, Y.F. Zhu, et al., *Int. J. Hydrogen Energ.* 45 (2020) 798–808.
- [34] C. Zhou, Z.Z. Fang, P. Sun, L. Xu, Y. Liu, *J. Power Sources* 413 (2019) 139–147.
- [35] X. Xiao, C. Xu, J. Shao, L. Zhang, T. Qin, et al., *J. Mater. Chem. A* 3 (2015) 5517–5524.
- [36] M. Calizzi, D. Chericoni, L.H. Jepsen, T.R. Jensen, L. Pasquini, *Int. J. Hydrogen Energ.* 41 (2016) 14447–14454.
- [37] M.S. Yahya, M. Ismail, *J. Energ. Chem* 28 (2019) 46–53.
- [38] L. Zhang, L. Chen, X. Fan, X. Xiao, J. Zheng, et al., *J. Mater. Chem. A* 5 (2017) 6178–6185.
- [39] M. Zhang, X. Xiao, X. Wang, M. Chen, Y. Lu, et al., *Nanoscale* 11 (2019) 7465–7473.
- [40] Y. Liu, H. Du, X. Zhang, Y. Yang, M. Gao, et al., *Chem. Commun.* 52 (2016) 705–708.
- [41] P. Yao, Y. Jiang, Y. Liu, C. Wu, K.-C. Chou, et al., *J. Magnes. Alloy* 8 (2020) 461–471.
- [42] L. Li, Z. Zhang, L. Jiao, H. Yuan, Y. Wang, *Int. J. Hydrogen Energ.* 41 (2016) 18121–18129.

- [43] L. Zhang, K. Wang, Y. Liu, X. Zhang, J. Hu, et al., *Nano Res* 14 (2020) 148–156.
- [44] J. Zhang, L. He, Y. Yao, X.J. Zhou, L.P. Yu, et al., *Renew. Energ.* 154 (2020) 1229–1239.
- [45] M. Chen, Y. Pu, Z. Li, G. Huang, X. Liu, et al., *Nano Res* 13 (2020) 2063–2071.
- [46] M. Avrami, *J. Chem. Phys.* 7 (1939) 1103–1112.
- [47] F. Jensen, *Qual. Reliab. Eng. Int.* 1 (1985) 13–17.
- [48] X. Yang, L. Ji, N. Yan, Z. Sun, X. Lu, et al., *Dalton Trans* 48 (2019) 12699–12706.
- [49] X. Zhang, Z. Leng, M. Gao, J. Hu, F. Du, et al., *J. Power Sources* 398 (2018) 183–192.
- [50] N. Patelli, A. Migliori, L. Pasquini, *ChemPhysChem* 20 (2019) 1325–1333.
- [51] L. Zhang, Z. Sun, Z. Cai, N. Yan, X. Lu, et al., *Appl. Surf. Sci.* 504 (2020) 144465.
- [52] C. Lu, J. Zou, X. Shi, X. Zeng, W. Ding, *Int. J. Hydrogen Energ.* 42 (2017) 2239–2247.
- [53] Y. Liu, J. Zou, X. Zeng, X. Wu, H. Tian, et al., *Int. J. Hydrogen Energ.* 38 (2013) 5302–5308.
- [54] W. Li, C. Li, H. Ma, J. Chen, *J. Am. Chem. Soc.* 129 (2007) 6710–6711.
- [55] Y. Wang, X. Chen, H. Zhang, G. Xia, D. Sun, et al., *Adv. Mater.* 32 (2020) 2002647.
- [56] L. Zhang, L. Ji, Z. Yao, N. Yan, Z. Sun, et al., *Int. J. Hydrogen Energ.* 44 (2019) 21955–21964.
- [57] K. Nogita, X.Q. Tran, T. Yamamoto, E. Tanaka, S.D. McDonald, et al., *Sci. Rep-UK* 5 (2015).
- [58] G. Xia, Y. Tan, X. Chen, D. Sun, Z. Guo, et al., *Adv. Mater.* 27 (2015) 5981–5988.
- [59] P. Rizo-Acosta, F. Cuevas, M. Latroche, *J. Mater. Chem. A* 7 (2019) 23064–23075.
- [60] X. Huang, X. Xiao, X. Wang, C. Wang, X. Fan, et al., *J. Phys. Chem. C* 122 (2018) 27973–27982.
- [61] M. Lotosky, R. Denys, V. A. Yartys, J. Eriksen, J. Goh, et al., *J. Mater. Chem. A* 6 (2018) 10740–10754.
- [62] L. Zhang, N. Yan, Z. Yao, Z. Sun, X. Lu, et al., *Int. J. Hydrogen Energ.* 52 (2020) 28134–28143.
- [63] J. Karst, F. Sterl, H. Linnenbank, T. Weiss, M. Hentschel, et al., *Sci Adv* 6 (2020), doi:10.1126/sciadv.aaz0566.